Bortezomib-Induced Muscle Toxicity in Multiple Myeloma

Valeria Guglielmi, PhD, Dominika Nowis, MD, PhD, Martina Tinelli, MD, Manuela Malatesta, PhD, Laura Paoli, MD, Matteo Marini, PhD, Paolo Manganotti, MD, PhD, Radoslaw Sadowski, PhD, Grzegorz M. Wilczynski, PhD, Vittorio Meneghini, MD, Giuliano Tomelleri, MD, and Gaetano Vattemi, MD, PhD

Abstract

Multiple myeloma (MM) accounts for ~13% of all hematologic malignancies. Bortezomib treatment is effective in MM, but can be complicated with neurological side effects. We describe a patient with symptomatic MM who had a reversible metabolic myopathy associated with bortezomib administration and pathologically characterized by excessive storage of lipid droplets together with mitochondrial abnormalities. In a single-center prospective study, 14 out of 24 patients with symptomatic MM were treated with bortezomib and, among these, 7 developed muscular signs and/or symptoms. The myopathy was characterized by a proximal muscle weakness involving lower limbs and was an early complication. Complete resolution of muscle weakness occurred after treatment discontinuation. Conversely, none of the patients who received a treatment without bortezomib developed muscular symptoms. Experimental studies demonstrate that in primary human myoblasts bortezomib at low concentrations leads to excessive storage of lipid droplets together with structural mitochondrial abnormalities, recapitulating the pathologic findings observed in patient's muscle. Our data suggest that patients treated with bortezomib should be monitored for muscular signs and/or symptoms and muscle weakness should alert the clinician to the possibility of myopathy. Bortezomib-induced metabolic myopathy is a potentially reversible entity with important implications for management and treatment of patients with MM.

Key Words: Bortezomib, Metabolic myopathy, Multiple myeloma, Muscle toxicity, Proteasome inhibitors.

From the Department of Neurosciences, Biomedicine and Movement Sciences, Section of Clinical Neurology, University of Verona, Verona, Italy (VG, MM, PM, GT, GV); Genomic Medicine, Department of General, Transplant and Liver Surgery, Medical University of Warsaw and Laboratory of Experimental Medicine, Centre of New Technologies, University of Warsaw, Warsaw, Poland (DN); Department of Medicine, Hematology Section, University of Verona, Verona, Italy (MT, LP, VM); Department of Neurosciences, Biomedicine and Movement Sciences, Section of Anatomy and Histology, University of Verona, Verona, Italy (MM); Department of Immunology, Center for Biostructure Research, Medical University of Warsaw, Warsaw, Poland (RS); and Laboratory of Molecular and Systemic Neuromorphology, Nencki Institute of Experimental Biology, Department of Neurophysiology Warsaw, Poland (GMW)

Send correspondence to: Gaetano Vattemi, MD, PhD, Department of Neurosciences, Biomedicine and Movement Sciences, Section of Clinical Neurology, University of Verona, P.le L.A. Scuro 10, 37134 Verona, Italy; E-mail: gaetano.vattemi@univr.it

Valeria Guglielmi and Dominika Nowis contributed equally to this work.

Financial support: This study was not supported, either partly or entirely, by any grant, fund, organization or corporation.

Conflict of interest: The authors have no duality or conflicts of interest to declare.

Supplementary Data can be found at http://www.jnen.oxfordjournals.org.

INTRODUCTION

Multiple myeloma (MM) is a malignant plasma cell disorder, characterized by bone marrow infiltration, production of a monoclonal protein, and induction of osteolysis (1, 2). The natural history of MM has profoundly changed with the introduction of novel drugs including thalidomide, lenalidomide, pomalidomide, and proteasome inhibitors (3). These treatments are complicated with various side effects potentially leading to early discontinuation of therapy. Therefore, the recognition and the management of potential toxic effects are crucial to provide an optimal therapeutic strategy and improve long-term outcomes (1, 2). The main known adverse effects associated with novel therapies include venous thromboembolism, myelosuppression, peripheral neuropathy, and gastrointestinal symptoms (4). Recent case reports raised the possibility of cardiac impairment due to bortezomib administration (5–7). However, there is no evidence of skeletal muscle toxicity induced by this drug. On the basis of the observation of a patient with symptomatic MM who developed muscle weakness after bortezomib treatment, we sought to undertake a prospective clinical study of a cohort of MM patients treated with systemic chemotherapy and an experimental study to evaluate the muscle toxicity of bortezomib in primary human muscle cell cultures.

MATERIALS AND METHODS

Case Report

A 65-year-old woman without any significant past medical history was diagnosed with MM, Durie-Salmon stage II and International Staging System stage II in March 2010 and was treated with bortezomib between September and December 2010 after discontinuation of prednisolone and thalidomide treatment due to side effects. Bortezomib was administered at 1.3 mg/m^2 on days 1, 4, 8, 11 of every 21-day

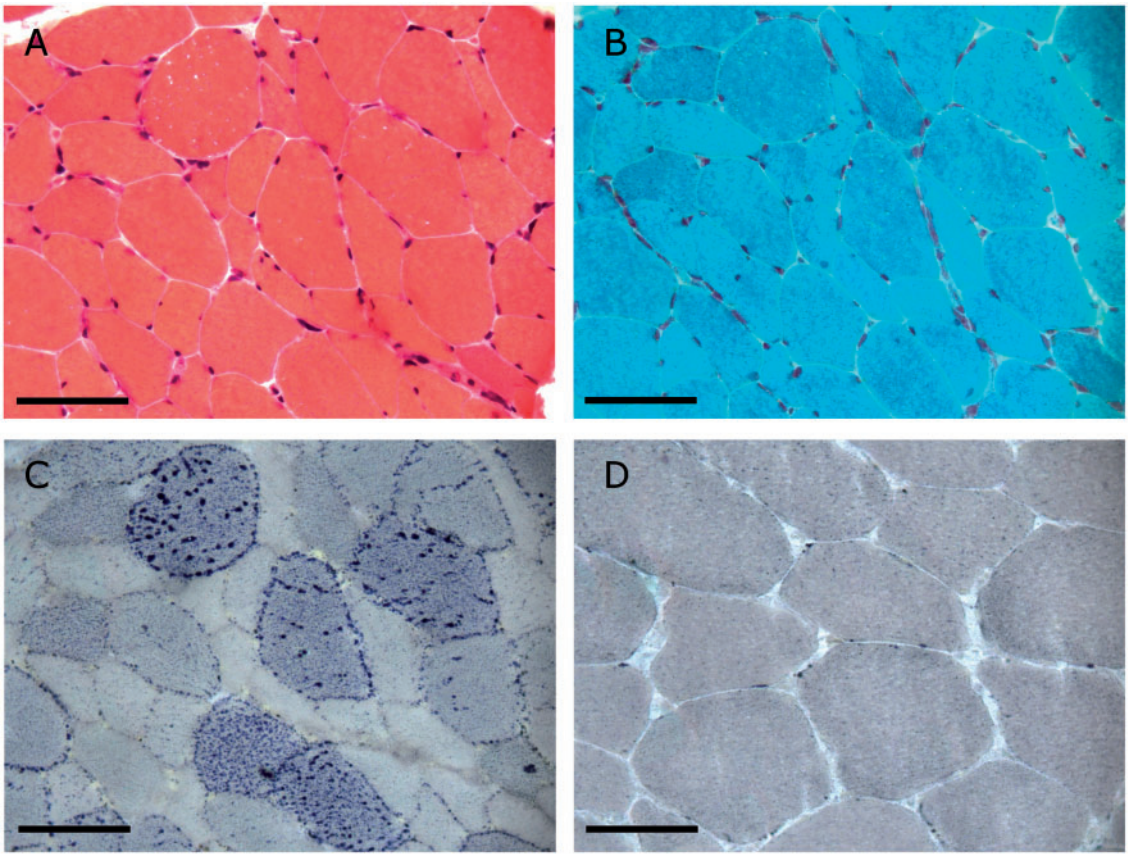

FIGURE 1. Morphological changes in skeletal muscle of a patient treated with bortezomib. Light microscopy of muscle biopsy cryosections. Hematoxylin and eosin stain shows fiber size variability **(A)** and modified Gomori trichrome reveals microvacuoles in muscle fibers **(B)**. Lipid droplets are increased within muscle fibers on Sudan black stain **(C)**. Sudan black staining of a control muscle biopsy **(D)**. Scale bars: 50 μm.

cycle. A few days after completing the third cycle, she referred a progressive proximal weakness of lower limbs. On clinical examination the patient squatted and rose from the floor with difficulty and weakness of the thigh flexors (grade 4/5 on the MRC scale) was present. Serum CK and nerve conduction studies were normal; needle electromyography recorded a myogenic pattern. A muscle biopsy of vastus lateralis, performed after informed consent, documented increased variation in fiber diameter with atrophic fibers belonged to both type 1 and 2 (Fig. 1A). Lipid droplets, detected with Sudan black (SB) staining and visible as microvacuoles on modified Gomori trichrome, were prominently increased within several muscle fibers (Fig. 1B–D; Supplementary Data Fig. S1). Neither necrotic nor regenerating muscle fibers were observed. All other histochemical staining including NADH-TR, COX, and SDH were normal. Ultrastructural examination confirmed the excessive storage of lipid droplets together with mitochondrial abnormalities consisting of swelling and *cristae* loss, and accumulation of normal-looking glycogen (Fig. 2A–C). Organic acid and acylcarnitine profiles, free and total carnitine, and enzymatic activities of the respiratory chain complexes were normal. Bortezomib was discontinued and other myeloma treatments were considered. Muscle weakness significantly improved in the following months and resolved based on data at last neurological follow-up in April 2013. The patient died due to disease progression on December 2014.

Patients

Between December 2010 and March 2012, 24 consecutive patients with symptomatic MM were prospectively evaluated at the Hematology Section of our Institution. In all patients demographic data, medical history, weight and height, Eastern Cooperative Oncology Group (ECOG) and Karnofsky performance status, diabetes mellitus, hypertension, and other significant co-morbidity were registered before starting treatment; MM characteristics (staging ISS and D&S, complete blood count, serum protein electrophoresis and immunofixation, creatinine, calcium, lactate dehydrogenase (LDH), β2-microglobulin serum levels, albumin, Bence Jones protein, plasma cell infiltration in the bone marrow) were recorded and skeleton X-ray was performed. Congo red staining of abdominal fat was assessed to detect amyloid deposits. Patients were treated according to International Myeloma Working Group (IMWG) guidelines and drugs dosage adjustments were made according to European Myeloma Network (EMN) recommendation. For each treatment line, data regarding the administered chemotherapy drugs were collected including specific

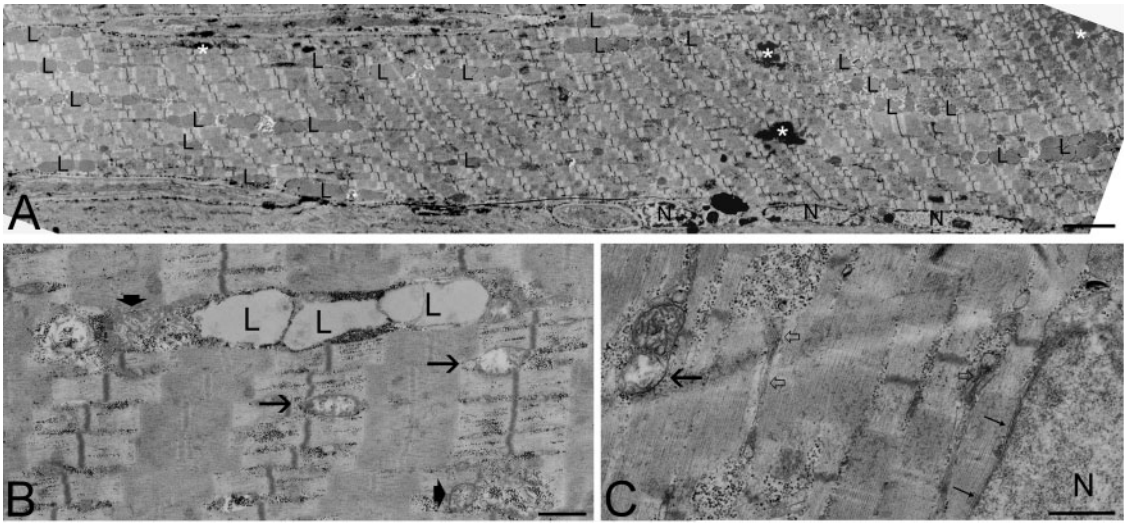

FIGURE 2. Ultrastructural changes in skeletal muscle of a patient treated with bortezomib. Transmission electron micrographs of skeletal muscle biopsy. **(A)** Low-magnification image (obtained as photo collage of 4 distinct micrographs) of a myofiber: Large amount of lipid droplets [L] and some glycogen clusters (asterisks) occurs among the microfibrils. N: Myonucleus. Scale bar: 5 μm. **(B, C)** Mitochondria showing empty matrix and short or absent cristae (arrows) and normal mitochondria (arrowheads) are present in the same myofibers. Lipid droplets [L] and scattered electron dense glycogen granules occur in the sarcoplasm. Note the well-preserved sarcoplasmic reticulum (open arrows) and nuclear envelope (thin arrows). N, myonucleus. Scale bars: 1 μm.

start and stop date for each drug given, number of cycles, cumulative dose, schedule modification during treatment and side effects. The response rates were measured using the IMWG criteria.

From April 2011 to April 2013 continuous neurological examination was performed in all patients by the same neurologist at baseline and every 2 cycles up to finishing the treatment. Peripheral neuropathy was graded according to the National Cancer Institute Common Terminology Criteria for Adverse Events (NCI CTCAE), v.2.0. Serum CK was determined in 12 patients. The institutional ethical committee approved the protocol and all monitored patients signed an informed consent.

Tissue Cultures

Primary cultures of normal human muscle were established as routinely performed in our laboratory (8). For differentiation into myotubes, myoblasts were grown at confluence and then shifted to medium without grown factors for 8 days. Experiments were done on 3 culture sets which were established from satellite cells derived from a portion of diagnostic vastus lateralis muscle biopsy of 3 different patients who ultimately were considered free of muscle diseases.

Cytotoxicity Assay

The cytotoxic effects of bortezomib on primary human myoblasts and myotubes were evaluated at different doses and drug exposure times. Cells were seeded in flat bottom 96-well plates at a density of 8×10^3 cells/well. Four wells for each treatment condition were seeded. Twenty-four hours after myoblasts seeding and, for myotubes, after 8 days of differentiation, the medium was changed and replaced by medium containing bortezomib at the final concentrations of 5, 10, 20, and 50 nM. After 24, 48, and 72 hours myoblasts were rinsed with PBS and stained with Trypan-blue. Two digital images were acquired for each well using a 40× objective (AxioCam HRc, Zeiss) and viable and nonviable cells were counted. After incubation, myotubes were harvested, stained with Trypan blue, and living and dead cells were counted under the hemocytomer chamber.

Sudan Black Staining

The histochemical staining was performed on primary myoblasts grown on coverslips and incubated with bortezomib at the final concentration of 5 nM for 3, 5, 7, and 9 days, and of 10 and 20 nM for 24 and 72 hours. Sudan black staining was also carried out on myotubes treated with bortezomib at the final dose of 5 nM for 5 and 7 days, and of 10 and 20 nM for 24 and 72 hours. The slides were incubated in a saturated Sudan black solution for 30 minutes at RT, washed twice with distilled water and mounted in a gelatin medium. Untreated cells were used as control.

Determination of Mitochondrial Membrane Potential Using JC-1 Staining

After treatment with bortezomib at the final concentration of 5 nM for 3, 5, 7, and 9 days, and of 10 and 20 nM for 24 and 72 hours, myoblasts were incubated in growth medium containing JC-1 (Molecular Probes) at the final concentration of 10 μ myoblasts minutes at 37 °C, 5% CO_2. Nuclei were counterstained with Hoechst 33342 dye (Molecular Probes)

TABLE 1. Baseline Characteristics of Multiple Myeloma Patients

Patient	Age	Gender	M-component	ISS	D&S	Amyloidosis	Line therapy	Treatment	Comorbidity
1	72	M	λ	3	3 A	No	1	MPT	No
2	60	M	IgGk	2	2 A	No	1	VTD	No
3	80	M	IgGk	2	2 B	No	2	VD	No
4	80	M	IgGk	2	3 A	No	1	MP	Yes
5	82	M	IgGk	2	3 A	No	2	VD	No
6	63	F	κ	3	3 A	No	1	MPV	No
7	47	M	IgGk	2	3 A	Yes	1	VD	No
8	75	F	IgAλ	3	3 B	No	1	MPV	No
9	57	M	IgGk	2	2 A	No	1	MPV	No
10	78	F	IgAk	3	3 B	No	2	VD	No
11	70	M	IgAλ	2	3 B	No	1	MPT	Yes
12	60	F	κ	3	3 B	No	1	VD	No
13	81	F	IgGλ	2	3 A	No	1	MPT	No
14	68	F	IgGk	2	3 A	No	1	MPT	No
15	80	M	IgGk	3	3 A	No	1	MPR	No
16	66	M	IgGλg	1	2 A	No	1	MPT	No
17	61	M	IgGk	3	3 B	No	1	VD	Yes
18	51	M	IgGk	3	2 B	No	1	VD	Yes
19	75	F	IgGk	2	2A	No	1	MPT	Yes
20	61	F	λ	1	2A	No	1	MPT	No
21	62	F	κ	3	3 B	No	1	VD	No
22	62	M	IgGk	3	2A	No	2	VD	Yes
23	71	M	IgGk	2	3 A	No	1	MPT	No
24	59	M	IgDλ	1	3 A	No	1	VTD	Yes

F: Female; M: Male; MPT: Melphalan, prednisone, thalidomide; VTD: Bortezomib, thalidomide, dexamethasone; VD: Bortezomib, dexamethasone; MP: Melphalan, prednisone; MPV: Melphalan, prednisone, bortezomib; MPR: Melphalan, prednisone, lenalidomide.

and samples were analyzed under Axiolab microscope (Zeiss). Untreated cells were used as control.

JC-1 (5,5′,6,6′-tetrachloro1,1′,3,3′-tetraethylbenzimidazolyl carbocyanine) is a nontoxic fluorescence probe that accumulates selectively in mitochondria in a potential-dependent manner, a process accompanied by a fluorescence emission shift from green to red. Mitochondrial membrane depolarization is indicated by a decrease in the red/green fluorescence intensity ratio.

Transmission Electron Microscopy

Ultrastructural examination was performed on myoblasts incubated with 5 nM bortezomib for 3, 5, 7, and 9 days. The cells were fixed with glutaraldehyde and embedded in epoxy resin as previously described (9). Mitochondrial area and extension of *cristae* were evaluated as detailed in Costanzo et al (10).

Immunoblot

Immunoblot analysis was performed on muscle tissues and on myoblasts that have been previously incubated with bortezomib at the final concentration of 5 nM for 3, 5, 7, and 9 days, and of 10 and 20 nM for 24 and 72 hours as detailed elsewhere (11). Briefly, myoblasts and 20-μm-thick frozen muscle sections were homogenized in RIPA buffer. Aliquots corresponding to 20 μg of total proteins were loaded on 10%T polyacrylamide gel and transferred to a nitrocellulose membrane. For immunoblotting, membranes were pre-hybridized with either 5% BSA, 0.05% Tween 20 in TBS (immunoblot for BiP) or with 10% nonfat dried milk in TBS (immunoblot for p62 and LC3) for 1 hour at RT and then incubated with the specific antibody diluted in either 5% BSA, 0.05% Tween 20 (BiP, Cell Signalling, dilution 1:1000) or in 5% nonfat dried milk in TBS (p62, BD Transduction Laboratories, dilution 1:1000; LC3, Cell Signalling, dilution 1:200) overnight at 4 °C. Bands were visualized with the ECL Advance Western Blotting Detection Kit (Amersham Pharmacia Biotech). Protein loading was confirmed by immunoblot with actin antibody (Sigma–Aldrich).

RT-PCR for X-Box-Binding Protein-1 Splicing

After incubation with bortezomib at the final concentration of 5 nM for 7 days, and 10 and 20 nM for 24 and 72 hours primary myoblasts were washed with PBS and lysed in TRIzol reagent (Invitrogen). Total RNA was isolated according to modified Chomczynski method. Concentration and purity of RNA were determined with a NanoDrop ND-2000c spectrophotometer (Thermo Scientific). For cDNA synthesis 1 μg of total RNA was used with oligo(dT) primer and Avian Myeloblastosis Virus (AMV) reverse transcriptase (all from EURx). PCR was performed using OneTaq 2 × Master Mix (NEB). Products of PCR amplification were analyzed by

TABLE 2. Patients Treated With Bortezomib

Patient	Treatment	Muscle impairment	Follow-up after treatment	CK	Other side effects
2	**Bortezomib 1.3 mg/mq day 1, 4, 8, 11**; DMS 20 mg day 1,4,8,11; Thal 100 mg/day (6 cycles)	No	No	Yes	No
3	**Bortezomib 1 mg/mq day 1, 8, 15, 22**; DMS 20 mg day 1, 15 (9 cycles)	No	No	No	Constipation
5	**Bortezomib 1 mg/mq day 1, 8, 15, 22;** DMS 20 mg day 1, 8, 15, 22 (8 cycles)	Yes	No	Yes	No
6	**Bortezomib 1,3mq/mq day 1, 8, 22, 29;** Melphalan 10 mg/mq day 1–4; Prednisone 75 mq day 1–4; (6 cycles)	No	No	Yes	Constipation
7	**Bortezomib 1.3 mg/mq day 1, 4, 8, 11;** DMS 20 mg day 1, 4, 8, 11 (3 cycles)	No	No	No	Renal failure, hypertension
8	**Bortezomib 1 mg/mq days 1, 8, 22, 29;** Melphalan 9 mg/mq days 1–4; Prednisone 50 mg/die days 1–4 (9 cycles)	Yes	Yes	Yes	Neutropenia
9	**Bortezomib 1 mq/mq day 1, 8, 22, 29;** Melphalan 8 mg/mq day 1–4; Prednisone 75 mq day 1–4 (9 cycles)	No	No	Yes	No
10	**Bortezomib 0.7 mg/mq day 1, 8, 15, 22;** DMS 20 mg day 1, 8, 15, 22 (9 cycles)	Yes	No	No	Peripheral neuropathy grade 1, constipation
12	**Bortezomib 1 mg/mq day 1, 8, 15, 22;** DMS 20 mg day 1, 8, 15, 22 (8 cycles)	Yes	Yes	Yes	Fever
17	**Bortezomib 1.3 mg/mq day 1, 4, 8, 11;** DMS 20 mg day 1, 4, 8, 11 (4 cycles)	No	Yes	No	No
18	**Bortezomib 1 mg/mq days 1, 4, 8, 11;** DMS 20 mg days 1, 4, 8, 11 (4 cycles)	Yes	No	Yes	Fever, cytomegalovirus infection, clostridium sepsis
21	**Bortezomib 1,3 mg/mq days 1, 8, 11, 22;** DMS 20 mg days 1, 8, 11, 22 (8 cycles)	Yes	No	No	Constipation
22	**Bortezomib 1 mg/mq day 1, 8, 15, 22;** DMS10 mg day 1, 8, 15, 22 (6 cycles)	No	No	No	No
24	**Bortezomib 1 mg/mq days 1, 4, 8, 11;** DMS 20 mg days 1, 4, 8, 11, Thal 100 mg/die (6 cycles)	Yes	Yes	No	Fever

DMS: Dexamethasone; Thal: Thalidomide.

electrophoresis in ethidium bromide stained 2% agarose gel, visualized under UV light and photographed using Alphaimager Mini (ProteinSimple). X-box-binding protein-1 (XBP1) mRNA is alternatively spliced to a product that differs in 26 bp from unspliced sequence (NCBI Reference Sequence: NM_001079539). The primers: XBP1 forward 5′-CCT TGT AGT TGA GAA CCA GG-3′ and XBP1 reversed—5′-GGG GCT TGG TAT ATA TGT GG-3′ allow for detection both unspliced and spliced XBP1.

Statistical Analysis

Statistical significance was determined by one-way analysis of variance. A level of statistical significance of at least 0.05 was adopted.

RESULTS

Patients

Patient demographics and disease characteristics of the 24 patients are listed in Table 1. Fourteen of 24 patients (58%) received at least 3 cycles of bortezomib and 7 of the 14 patients (50%) receiving bortezomib treatment experienced muscle weakness (Table 2). In the 7 patients muscle weakness was symmetrical and involved proximal lower limb muscles, in particular thigh flexor muscles; in 6 of them muscular symptoms appeared within the first 2 cycles and in 1 patient within the first 4 cycles. At follow-up evaluation during treatment, the weakness has not worsened and remained confined to the lower limbs in all patients. Three of the 7 patients had a follow-up after treatment, resolution of muscle weakness occurred after bortezomib was discontinued. None of the remaining 10 patients (42%) who received a treatment without bortezomib developed muscular signs and/or symptoms. One of the 14 patients receiving bortezomib treatment developed a sensory polyneuropathy of grade 1, clinically characterized by paresthesias in the distal lower limbs and distally reduced vibratory sensation up to the knees. Serum CK, available in twelve patients of which 7 received bortezomib, was normal.

Bortezomib Exerts Cytotoxic Effects in Primary Human Myoblasts

Bortezomib reduced survival of human myoblasts grown in vitro. These effects were time- and dose-dependent and were observed after 24 hours of treatment starting at 10 nM concentrations, which are within the range inducing cytotoxic effects in human tumor cells (Fig. 3A). Primary human myotubes displayed a decreased survival after 72 hours of treatment with 20 and 50 nM concentrations of bortezomib. No statistically significant difference in myotubes' survival was reported for the other times and doses of treatment (Supplementary Data Fig. S2).

Bortezomib at Low Concentrations (5 nM) Leads to Lipid Accumulation Associated With Mitochondrial Impairment

SB staining, which detects neutral lipids and complex lipids and lipoproteins as well, revealed a remarkable and

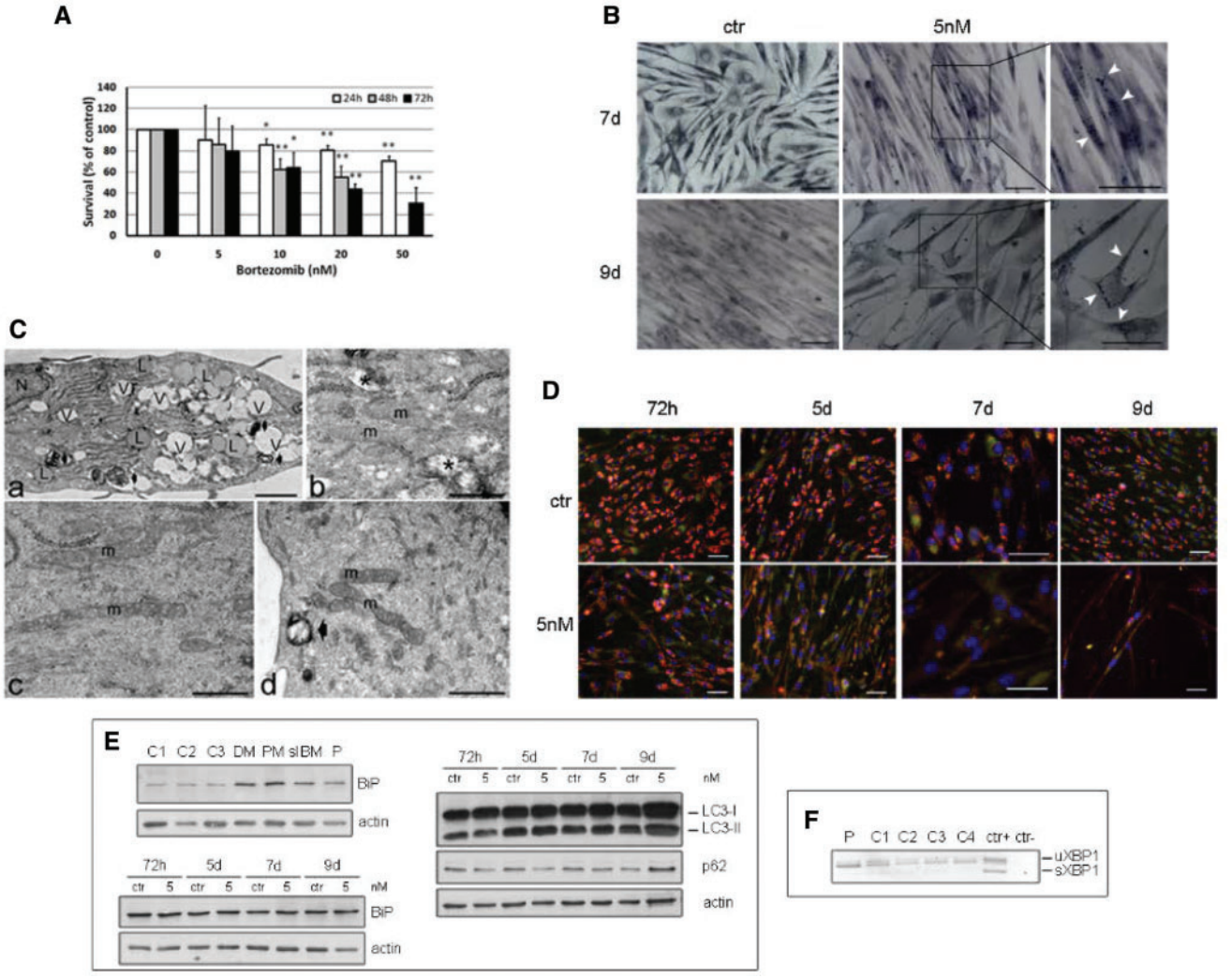

FIGURE 3. Cytotoxicity and biological effects of bortezomib in primary human myoblasts. **(A)** Cytotoxic/cytostatic effect of bortezomib on primary human myoblasts. Primary human myoblasts were exposed for 24, 48, or 72 hours to the indicated concentrations of bortezomib. The cytostatic/cytotoxic effects were evaluated with Trypan blue staining. The number of vital cells are expressed as percentage of cells in respect to untreated control (mean ± SD); *$p < 0.05$ vs untreated control; **$p < 0.01$ vs untreated control. **(B)** Sudan black staining on primary human myoblasts shows a prominent increasing in lipid accumulation after 7 and 9 days of treatment with 5 nM bortezomib. Scale bars: 50 μm. Transmission electron micrograph of human myoblasts in vitro. **(C)**. Cells treated with 5 nM bortezomib for 9 days **(a, b)** show accumulation of lipid droplets [L], vacuoles [V], and residual bodies (arrow); moreover, some mitochondria appear as swollen with clear matrix and blurred cristae (asterisks), while normal mitochondria [m] are characterized by a few cristae. N: Nucleus. Control cells show mitochondria [m] with well-developed cristae both at 3 **(c)** and 9 **(d)** days of culture; only a few vacuoles and residual bodies (arrow) occur after 9 days. Scale bars: 2 μm **(a)**; 0.5 μm **(b–d)**. **(D)** Fluorescence microscopy analysis after JC-1 staining revealed a red (polarized mitochondria) to green (depolarized mitochondria) shift in JC-1 fluorescence emission in primary human myoblasts that have been treated with 5 nM of bortezomib. Mitochondria depolarization is remarkable after 7 and 9 days of treatment. Scale bars: 50 μm. **(E)** Western blot analysis documented no changes in the expression levels of BiP in skeletal muscle of a patient treated with bortezomib [P] as compared with 3 different control subjects (C1, C2, and C3) and in primary human myoblasts treated with bortezomib at 5 nM after 3, 5, 7, and 9 days as compared with untreated controls. Muscle biopsy of a patient affected by dermatomyositis (DM), polymyositis (PM), and sporadic inclusion body myositis (sIBM) were used as positive control of increased BiP expression as the result of ER stress. Immunoblot analysis revealed similar expression levels of p62 and LC3I/LC3II in primary human myoblasts treated with bortezomib at 5 nM for 3, 5, 7, and 9 days and untreated controls. **(F)** RT-PCR failed to detect the unconventional splicing of the XBP1 in muscle of patient [P] and of 4 different control subjects (C1, C2, C3, and C4).

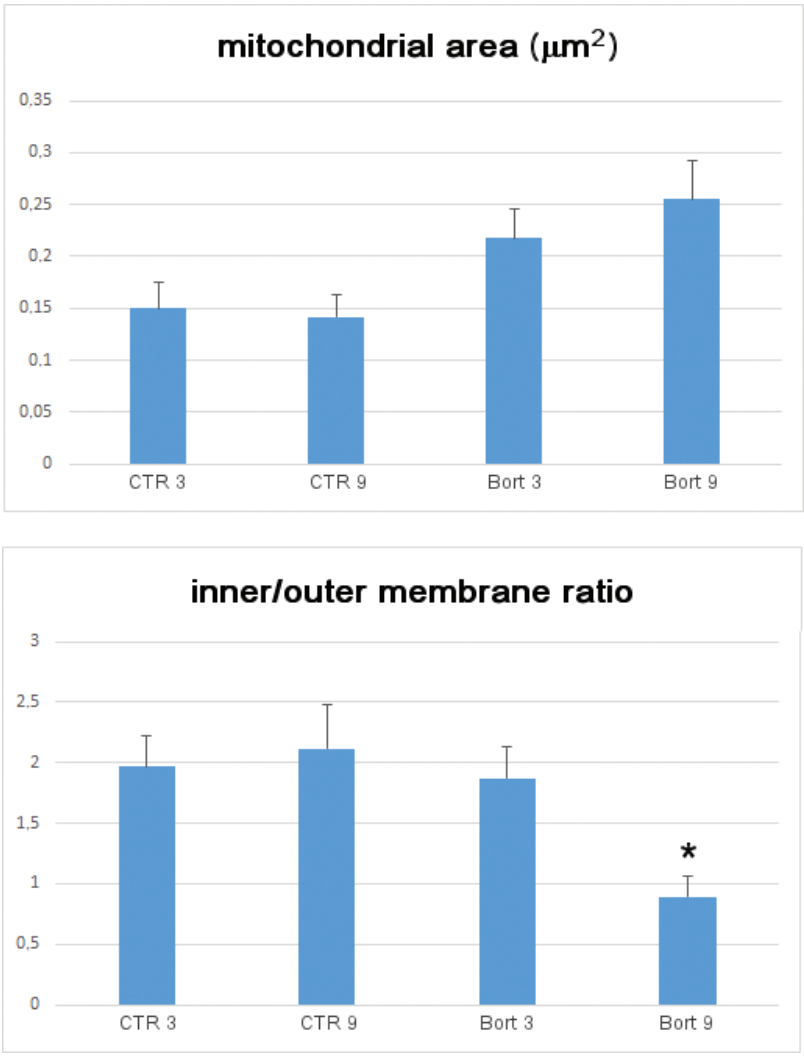

FIGURE 4. Mitochondrial area and extension of *cristae* in primary human myoblasts. Mean ± SE values (n = 40) of mitochondrial area and inner/outer membrane ratio (estimating the extension of cristae independently of mitochondrial size) in human myoblasts treated with 5 nM bortezomib for 3 and 9 days as well as in the respective controls (CTR). Mitochondrial cristae length significantly decreases in myoblasts treated with bortezomib for 9 days (asterisk); no difference has been found for mitochondrial area.

increasing accumulation of lipids within the myoblasts starting at 7 days of incubation with bortezomib at 5 nM concentration. Lipid droplets increased in a time-dependent manner involving most of myoblasts after 9 days of treatment (Fig. 3B). Ultrastructural analysis documented some lipid globules in a very few bortezomib-treated muscle cells at 72 hours. At 9 days of treatment lipids were detected in the form of droplets of variable size, not membrane-bound and randomly distributed in the cytoplasm (Fig. 3C). In addition, several mitochondria with structural abnormalities including swelling and loss of *cristae* were observed at 7 and 9 days of incubation (Fig. 3C), while morphologically undamaged mitochondria showed a significant decrease in the inner membrane length (Fig. 4). JC-1 staining, performed to evaluate whether bortezomib could affect the mitochondrial membrane potential, revealed a red (polarized mitochondria) to green (depolarized mitochondria) shift in the fluorescence emission in primary human myoblasts incubated with 5 nM of bortezomib for 3, 5, 7, and 9 days. At days 7 and 9 the red fluorescence was barely detectable, suggesting that nearly all mitochondria were depolarized (Fig. 3D).

Proteasome inhibition by bortezomib has been associated with the modulation of several biological events including the endoplasmic reticulum (ER) stress and the autophagy. Therefore, we determined the levels of BiP and XBP1 mRNA for ER stress, and of the LC3 and p62, proteins for autophagy. Similar expression levels of BiP and the absence of the unconventional splicing of the XBP1 were observed both in muscle of patient and of control subjects and in primary human myoblasts incubated with bortezomib at 5 nM after 3, 5, 7, and 9 days (Figs. 3E–F, 5D; Supplementary Data Fig. S3). Immunoblot analysis documented no changes in p62 and LC3I/LC3II

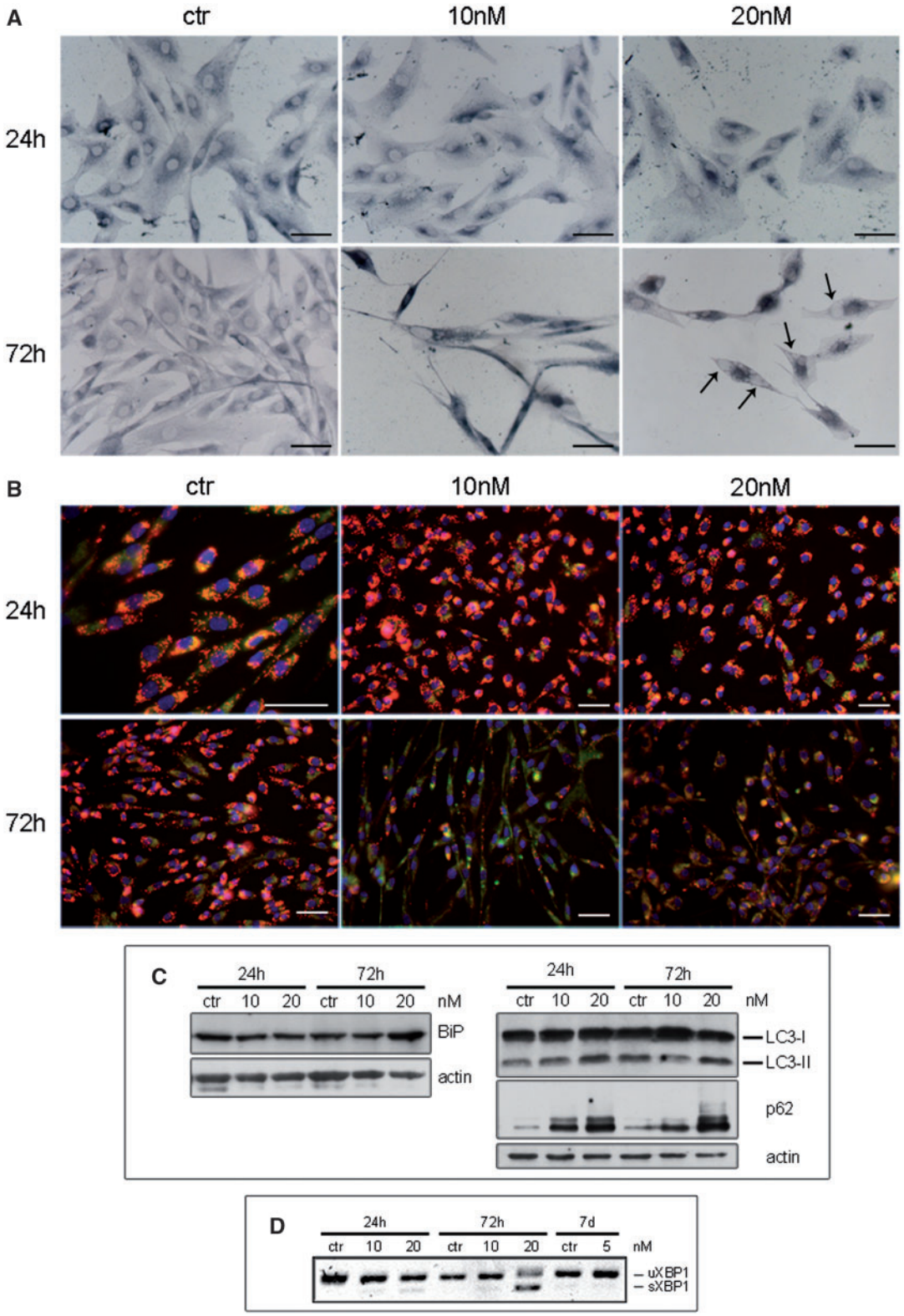

FIGURE 5. Biological effects of bortezomib at high concentrations in primary human myoblasts. **(A)** Sudan black staining on primary human myoblasts after 24 and 72 hours of treatment with bortezomib at 10 and 20 nM concentrations did not reveal lipid accumulation. A remarkable cytosolic vacuolization was visible after 72 hours incubation with 20 nM bortezomib (arrows). Scale bars: 50 μm. **(B)** Fluorescence microscopy analysis after JC-1 staining documented a red (polarized mitochondria) to green (depolarized mitochondria) shift in JC-1 fluorescence emission in primary human myoblasts treated with 10 and 20 nM of

expression in primary human myoblasts incubated with bortezomib at 5 nM for 3, 5, 7, and 9 days (Fig. 3E; Supplementary Data Fig. S3).

SB staining of myotubes treated with bortezomib at 5 nM after 5 and 7 days revealed no changes in lipid content (Supplementary Data Fig. S4).

Bortezomib at High Concentrations (10 and 20 nM) Induces ER Stress and Affects Autophagy Function

Examination of the primary human myoblasts by light microscopy showed that a 72-hour incubation with bortezomib leads to a prominent cytosolic vacuolization, especially at the highest 20 nM concentration (Fig. 5A). After 24- and 72-hour incubations with 10 and 20 nM bortezomib, SB staining documented no excess content of lipids in the cytoplasm of myoblasts and myotubes (Fig. 5A; Supplementary Data Fig. S4). In human myoblasts incubated for 24 hours with bortezomib at 10 and 20 nM concentrations a remarkable red fluorescence emission of JC-1 was observed without any difference as compared with the untreated cells suggesting that bortezomib does not affect mitochondrial membrane potential at these concentrations and duration of treatment (Fig. 5B). However, after 72 hours of incubation a decrease of red fluorescence was observed after 10 and 20 nM of bortezomib as compared with untreated cells and was accompanied by the increase of the green fluorescence in the cytoplasm (Fig. 5B).

Incubation of muscle cells with 20 nM of bortezomib for 72 hours led to increased expression of BiP (Fig. 5C; Supplementary Data Fig. S3). In addition, myoblasts incubated with 20 nM bortezomib for 24 and 72 hours presented the unconventional splicing of XBP1 (Fig. 5D). In immunoblot analysis, the amount of LC3II was increased in primary human myoblasts following a 24- and 72-hour exposure to 20 nM bortezomib (Fig. 5C; Supplementary Data Fig. S3); accompanied by a progressive increase in the expression levels of p62 (Fig. 5C; Supplementary Data Fig. S3).

DISCUSSION

Several lines of evidence suggest that muscle disorder in our patient was induced by bortezomib. First, muscle weakness developed while the patient was treated with therapeutic doses of bortezomib. Second, other possible causes for myopathy were ruled out and no other drugs with a probable myotoxic effect, except for steroid, were administered at that time. Last, the withdrawal of bortezomib was followed by a complete resolution of symptoms. It is unlikely that the muscle toxicity was glucorticoid-induced given that the patient after bortezomib discontinuation was switched to other myeloma treatments containing corticosteroids. In addition histopathological features of muscle biopsy did not point to iatrogenic steroid myopathy that is usually characterized by selective atrophy of type 2 fast-twitch fibers, mainly type 2B, without lipid accumulation within muscle fibers.

Although there are no studies in which is reported a toxicity of the drug on skeletal muscle tissue, our clinical observation strongly suggests that bortezomib treatment can affect muscle function. To address this issue, we evaluated the frequency and characteristics of muscle involvement in 24 consecutive patients with symptomatic MM treated at Hematology Section of our Institution by a single-center prospective study conducted between December 2010 and March 2012. In our study, 14 out of 24 patients (58%) with symptomatic MM were treated with bortezomib and, among these, 7 (50%) developed muscular signs and/or symptoms. In all 7 patients the myopathy was characterized by a proximal muscle weakness involving lower limbs and was an early complication when it occurred, usually within the first 2 cycles of therapy. Complete resolution of muscle weakness occurred after treatment discontinuation in patients with longer follow-up indicating the potential reversibility of the myopathy. Conversely, none of the 10 patients who received a treatment without bortezomib developed muscular symptoms.

The mechanism of muscle injury associated with bortezomib remains to be elucidated. In our patient a metabolic myopathy consisting of lipid accumulation within muscle fibers was documented. The presence of mitochondrial abnormalities at ultrastructural level suggests that lipid deposits in muscle can be secondary to mitochondrial dysfunction; the absence of abnormalities in the organic acid and acylcarnitine profiles as well as in the free and total carnitine levels rules out other causes of lipid storage myopathy. Clearly it is a shortcoming that we have no muscle biopsy data beyond the index patient, but we considered no ethical and correct to perform muscle biopsy in the other patients because preliminary data suggested the potential reversibility of the symptoms, as it was later confirmed by our clinical study.

We then investigated the direct effect of bortezomib on primary human myoblasts. Our study demonstrated that human muscle cells exhibited a dose- and time-dependent decrease in cell viability only in response to relative high concentrations of bortezomib (10 and 20 nM). Bortezomib used at 5 nM, which is the range of plasma concentration following administration of 1.3 mg/m^2 in patients (12, 13), did not

FIGURE 5. Continued
bortezomib for 72 hours. No detectable mitochondria depolarization was observed after 24 hours of incubation with bortezomib at 10 and 20 nM concentration. Scale bars: 50 μm. **(C)** Western blot analysis in primary human myoblasts reported an increased expression levels of BiP after 72 hours of treatment with bortezomib 20 nM concentration and the increased amount of LC3II following incubation with bortezomib at 20 nM for 24 and 72 hours. A progressive increase in p62 protein expression was observed after the exposure to 10 and 20 nM of bortezomib for 24 and 72 hours. **(D)** RT-PCR detected the unconventional splicing form of XBP1 (sXBP1) as consequence of treatment with bortezomib at 20 nM concentration for 24 and 72 hours.

induce cytotoxic effects, but led to excessive storage of lipid droplets together with structural mitochondrial abnormalities in primary human myoblasts, recapitulating the pathologic findings that have been observed in muscle of our patient. Although an effect of bortezomib on mitochondria has been previously described (14–6), the intracellular accumulation of lipids as a pathological feature of drug treatment is reported in the present study for the first time. It is noteworthy that patients with bortezomib-induced peripheral neuropathy have alterations in expression profile of genes that might have an involvement in mitochondrial changes and in particular the enzyme coding gene *CPT1C* which is involved in lipid metabolism and consequently in the formation of lipid droplets (17). The complex relationship between lipid accumulation and mitochondrial dysfunction is well documented in literature; alterations in number and/or structure of mitochondria may lead to lipid storage, but it has also been observed that excessive lipid droplets may cause mitochondrial abnormalities (18). We reported that after 72 hours of treatment with bortezomib many myoblasts displayed loss of mitochondrial potential whereas only some lipid droplets in a very few cells were visible at ultrastructural level. Although it is not possible to establish unambiguously if the increase in the lipid content causes or is due to mitochondrial dysfunction, our findings could suggest that lipid accumulation is secondary to a defect in mitochondrial function.

One of the molecular mechanisms at the basis of the therapeutic efficacy of bortezomib is the induction of ER stress as a consequence of the inhibition of the 26S proteasome activity (19, 20). In the present study we found that bortezomib induces ER-stress in primary human myoblasts only at higher concentrations (10 or 20 nM), as demonstrated by the upregulation of BiP protein and the alternative splicing of XBP-1, but not at 5 nM concentration where the abnormal accumulation of lipids and mitochondrial damage were already observed. Our findings suggest that the effects on mitochondrial morphology and function as well as on lipid storage are not the consequence of ER stress.

In the literature contrasting findings have been reported on the effect of bortezomib on the autophagic flux. A stimulatory action has been documented in some papers whereas others studies described the blockage of the autophagic function (21–7). The increased expression of p62 and of LC3II, 2 protein markers for detecting the autophagic flux, and the morphologic features of extensive cytosolic vacuolization clearly documented that high concentrations of bortezomib affects the catabolic process of autophagy in primary human myoblasts.

Lastly, we evaluated the cytotoxic effect of bortezomib on primary human myotubes. Our study demonstrated that myotubes are less susceptible to bortezomib than myoblasts, showing a decrease in cell viability only after 72 hours of treatment with high concentrations of drug (20 and 50 nM). Moreover, myotubes treated with bortezomib did not display changes in lipid content.

In conclusion, clinicians should be aware of the existence of bortezomib-induced metabolic myopathy, a potentially reversible entity with important implications for management and treatment of patients with MM. Patients treated with bortezomib should be carefully monitored by a neurologist for muscular signs and/or symptoms and muscle weakness should alert the clinician to the possibility of myopathy.

REFERENCES

1. Rollig C, Knop S, Bornhauser M. Multiple myeloma. Lancet 2015;385: 2197–208
2. Vincent Rajkumar S. Multiple myeloma: 2014 update on diagnosis, risk-stratification, and management. Am J Hematol 2014;89: 999–1009
3. Kumar SK, Rajkumar SV, Dispenzieri A, et al. Improved survival in multiple myeloma and the impact of novel therapies. Blood 2008;111: 2516–20
4. Mateos MV. Management of treatment-related adverse events in patients with multiple myeloma. Cancer Treat Rev 2010;36(Suppl. 2):S24–32
5. Voortman J, Giaccone G. Severe reversible cardiac failure after bortezomib treatment combined with chemotherapy in a non-small cell lung cancer patient: a case report. BMC Cancer 2006;6:129
6. Enrico O, Gabriele B, Nadia C, et al. Unexpected cardiotoxicity in haematological bortezomib treated patients. Br J Haematol 2007;138: 396–7
7. Hacihanefioglu A, Tarkun P, Gonullu E. Acute severe cardiac failure in a myeloma patient due to proteasome inhibitor bortezomib. Int J Hematol 2008;88:219–22
8. Askanas V, Engel WK. A new program for investigating adult human skeletal muscle grown aneurally in tissue culture. Neurology 1975;25: 58–67
9. Malatesta M, Giagnacovo M, Cardani R, et al. Human myoblasts from skeletal muscle biopsies: in vitro culture preparations for morphological and cytochemical analyses at light and electron microscopy. Methods Mol Biol 2013;976:67–79
10. Costanzo M, Cisterna B, Vella A, et al. Low ozone concentrations stimulate cytoskeletal organization, mitochondrial activity and nuclear transcription. Eur J Histochem 2015;59:2515
11. Guglielmi V, Vattemi G, Gualandi F, et al. SERCA1 protein expression in muscle of patients with Brody disease and Brody syndrome and in cultured human muscle fibers. Mol Genet Metab 2013;20:00261–8
12. Leveque D, Carvalho MC, Maloisel F. Review. Clinical pharmacokinetics of bortezomib. In Vivo 2007;21:273–8
13. Reece DE, Sullivan D, Lonial S, et al. Pharmacokinetic and pharmacodynamic study of two doses of bortezomib in patients with relapsed multiple myeloma. Cancer Chemother Pharmacol 2011;67:57–67
14. Cavaletti G, Gilardini A, Canta A, et al. Bortezomib-induced peripheral neurotoxicity: a neurophysiological and pathological study in the rat. Exp Neurol 2007;204:317–25
15. Shin YK, Jang SY, Lee HK, et al. Pathological adaptive responses of Schwann cells to endoplasmic reticulum stress in bortezomib-induced peripheral neuropathy. Glia 2010;58:1961–76
16. Nowis D, Maczewski M, Mackiewicz U, et al. Cardiotoxicity of the anticancer therapeutic agent bortezomib. Am J Pathol 2010;176: 2658–68
17. Broyl A, Corthals SL, Jongen JL, et al. Mechanisms of peripheral neuropathy associated with bortezomib and vincristine in patients with newly diagnosed multiple myeloma: a prospective analysis of data from the HOVON-65/GMMG-HD4 trial. Lancet Oncol 2010;11: 1057–65
18. Chow L, From A, Seaquist E. Skeletal muscle insulin resistance: the interplay of local lipid excess and mitochondrial dysfunction. Metabolism 2010;59:70–85
19. Obeng EA, Carlson LM, Gutman DM, et al. Proteasome inhibitors induce a terminal unfolded protein response in multiple myeloma cells. Blood 2006;107:4907–16
20. Argyriou AA, Iconomou G, Kalofonos HP. Bortezomib-induced peripheral neuropathy in multiple myeloma: a comprehensive review of the literature. Blood 2008;112:1593–9
21. Jaganathan S, Malek E, Vallabhapurapu S, Driscoll JJ. Bortezomib induces AMPK-dependent autophagosome formation uncoupled from apoptosis in drug resistant cells. Oncotarget 2014;5:12358–70
22. Min H, Xu M, Chen ZR, et al. Bortezomib induces protective autophagy through AMP-activated protein kinase activation in cultured pancreatic and colorectal cancer cells. Cancer Chemother Pharmacol 2014;74: 167–76

23. Lou Z, Ren T, Peng X, et al. Bortezomib induces apoptosis and autophagy in osteosarcoma cells through mitogen-activated protein kinase pathway in vitro. J Int Med Res 2013;41:1505–19
24. Selimovic D, Porzig BB, El-Khattouti A, et al. Bortezomib/proteasome inhibitor triggers both apoptosis and autophagy-dependent pathways in melanoma cells. Cell Signal 2013;25:308–18
25. Laussmann MA, Passante E, Dussmann H, et al. Proteasome inhibition can induce an autophagy-dependent apical activation of caspase-8. Cell Death Differ 2011;18:1584–97
26. Periyasamy-Thandavan S, Jackson WH, Samaddar JS, et al. Bortezomib blocks the catabolic process of autophagy via a cathepsin-dependent mechanism, affects endoplasmic reticulum stress and induces caspase-dependent cell death in antiestrogen-sensitive and resistant ER+ breast cancer cells. Autophagy 2010;6: 19–35
27. Kao C, Chao A, Tsai CL, et al. Bortezomib enhances cancer cell death by blocking the autophagic flux through stimulating ERK phosphorylation. Cell Death Dis 2014;5:e1510